NJC

PAPER

View Article Online
View Journal | View Issue

Check for updates

Cite this: *New J. Chem.*, 2020, **44**, 2941

Enhancing the anti-corrosion performance of ZIF-8-based coatings *via* microstructural optimization†

Mu Zhang and Yi Liu *

Received 3rd December 2019,
Accepted 20th January 2020

DOI: 10.1039/c9nj05998a

rsc.li/njc

Although still in their infancy, MOF-based coatings have shown great potential for their applications as anti-corrosion coatings. Nevertheless, an in-depth investigation of the influence of morphology on their anti-corrosion performance has rarely been conducted. In this study, ZIF-8-based anti-corrosion coatings with diverse microstructures were prepared by the facile hydrothermal growth of ZnAl–NO_3 LDH buffer layers followed by solvothermal treatment with ZIF-8 precursor solutions with different recipes. DC polarization tests demonstrated that the precursor solution containing only 2-methylimidazole led to the formation of ZIF-8–ZnAl–NO_3 LDH composite coatings with superior anti-corrosion performances probably due to the reduced grain boundary defect density.

Introduction

The corrosion of metals and their alloys will result in severe economic and safety issues. Chromate-containing conversion coatings, which have historically been considered as an effective anti-corrosion method for metallic substrates, have been restricted because of their toxic and carcinogenic properties.[1–3] Therefore, new anti-corrosion materials with excellent anti-corrosion performance, easy processability, low manufacturing cost and improved sustainability are yet to be developed. Among various materials, layered double hydroxides (LDHs) provide a cost-effective and eco-friendly way to protect metals (like Al) against corrosion.[4–7] For instance, laurate-intercalated ZnAl LDH films involving *in situ* hydrothermal growth and anion exchange with laurate have been prepared. The prepared LDH film exhibited low current density ($\sim 10^{-9}$ A cm^{-2}) in a DC polarization test.[4] A recent study further indicated that the prepared ZnAl–NO_3 LDH films not only acted as anti-corrosive coatings but were also involved in a self-healing process *via* the dissolution–recrystallization mechanism when exposed to a chloride-containing environment.[5]

Besides LDHs, diverse hydrophobic, water-stable and small pore-sized MOF materials (such as dopamine-grafted-MOF-5,[8] $[ZnC_{12}C_{16}]$,[9] ZIF-8,[10,11] ZIF-90,[12] Mg-MOF-74,[13] Ag-MOFs,[14] $M(4\text{-}SO_3\text{-}pzH)_n$,[15] $LnPc_2$[16] and phosphonate-based MOF[17]) have been prepared that exhibit unprecedented opportunities for anti-corrosion applications. For example, we recently synthesized well-intergrown ZIF-8 coatings on Al plates with excellent anti-corrosion performances by facile solvothermal growth.[11] Nevertheless, to date, the effect of the microstructures of most MOF-based coatings on their anti-corrosion performance has not been well elucidated.

To further improve their anti-corrosion performance, MOF coatings should be well-intergrown, continuous, and firmly attached to the metal surface. In addition, the fabrication process should be simple, cost-effective and eco-friendly. Herein, we developed a facile approach to prepare ZIF-8-based anti-corrosion coatings with different microstructures by the simple solvothermal conversion of ZnAl–NO_3 LDH buffer layers with different recipes. Under hydrothermal conditions, the surface of Al plates was partially reduced and Al^{3+} was released to the precursor solution; simultaneously, NO_3^- charge compensating anions were spontaneously intercalated into the interlayer galleries of ZnAl brucite-like sheets.[18–20] Consequently, the ZnAl–NO_3 LDH buffer layers were subjected to solvothermal treatment in a methanol solution containing 2-mIm (in some cases, additional $Zn(NO_3)_2 \cdot 6H_2O$ was added), which not only served as the organic linker of ZIF-8, but also promoted the dissolution of the ZnAl–NO_3 LDH buffer layers *via* nucleophilic attack. Finally, the released Zn^{2+} coordinated with 2-mIm, leading to the formation of well-intergrown ZIF-8 coatings on Al plates. It should be noted that prolonging the reaction time resulted in a gradual decrease in the grain boundary defects in ZIF-8 coatings. After the formation of defect-free protective ZIF-8 surface coatings, further nucleophilic attack of 2-mIm underneath the ZnAl–NO_3 LDH buffer layers was effectively

---

State Key Laboratory of Fine Chemicals, School of Chemical Engineering, Dalian University of Technology, No. 2 Linggong Road, Ganjingzi District, Dalian, 116024, P. R. China. E-mail: diligenliu@dlut.edu.cn

† Electronic supplementary information (ESI) available. See DOI: 10.1039/c9nj05998a

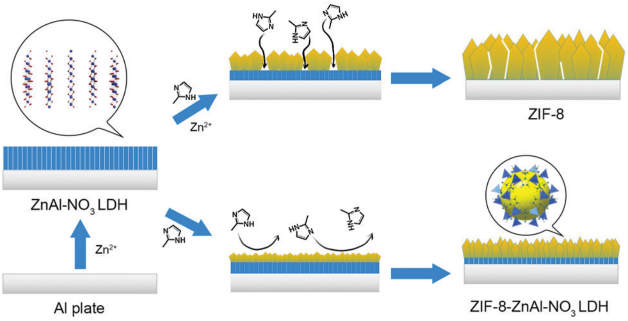

Fig. 1 Schematic illustration for the modification of ZIF-8 anti-corrosion coatings on Al plates by the hydrothermal conversion of ZnAl–NO_3 LDH precursor coatings under two different solvothermal conditions.

prevented, ultimately leading to the formation of the ZIF-8–ZnAl–NO_3 LDH composite coatings (schematically shown in Fig. 1). The prepared ZIF-8 coatings were subjected to DC polarization tests for the quantitative evaluation of their anti-corrosion performance. It was found that the microstructure of the MOF-based coatings exerted a significant influence on their anti-corrosion performance.

Experimental

Materials and instruments

$Zn(NO_3)_2·6H_2O$ (99.0 wt%, Shanghai Makclin Biochemical), NH_4NO_3 (98.0 wt%, Shanghai Makclin Biochemical), Al plate (99.9 wt%, Shenyang Chemicals), chemical communication, methanol (99.5 wt%, Tianjin Damao Chemicals), 2-methylimidazole (2-mIm, 98 wt%, Energy Chemicals), ammonium hydroxide (1 wt%, diluted from 25 wt%, Shenyang Chemicals), sodium formate (99.5 wt%, Shanghai Makclin Biochemical) were used as received.

SEM images of the samples were recorded using field-emission-SEM (SUPARR 55, ZEISS) at an acceleration voltage of 3 kV. XRD patterns to identify the LDH and ZIF-8 samples were obtained using an X-ray diffractometer (SmartLab 9 kW, Rigaku Corporation) with the monochromatic Cu radiation. A Fourier infrared spectrometer (FT-IR, EQUINOX55, BRUKER) was used to determine the infrared spectra of the ZIF-8 coatings as a basis for determining the density of grain boundary defects on the surface of the film. An electrochemical analyzer (CHI-660E, CH Instruments) was used to evaluate the corrosion resistance of coatings.

Growth of ZnAl–NO_3 LDH buffer layers on bare Al substrates

Prior to use, the Al substrate was sanded with a sandpaper and then thoroughly cleaned by ultrasonic cleaning with deionized water. ZnAl–NO_3 LDH buffer layer with optimized microstructures was prepared by mixing 4.5 g $Zn(NO_3)_2·6H_2O$ and 4.8 g NH_4NO_3 in 100 ml DI water. Consequently, 7 ml $NH_3·H_2O$ (1 wt%) was slowly added into the precursor solution in an ice bath with vigorous stirring. After further stirring for 30 min at room temperature, the bare Al plate was vertically placed in a 50 ml Teflon-lined stainless vessel. After the hydrothermal reaction at 40 °C for 36 hours, the vessel was taken out and naturally cooled to room temperature in air.

Preparation of ZIF-8–ZnAl–NO_3 LDH coatings

The precursor solution was prepared by mixing 1.0 g of 2-mIm in 50 ml methanol. Then, the ZnAl–NO_3 LDH buffer layer-modified Al plate was vertically placed in a 50 ml Teflon-lined stainless vessel. After a solvothermal reaction at 80 °C for 36 hours, the vessel was taken out and cooled to room temperature in air.

Preparation of ZIF-8 coatings

The precursor solution was prepared by mixing 0.49 g of 2-mIm, 0.54 g of $Zn(NO_3)_2·6H_2O$ and 0.27 g of sodium formate in 80 ml methanol. The ZnAl–NO_3 LDH buffer layer-modified Al plate was vertically placed in a 50 ml Teflon-lined stainless vessel. After the solvothermal reaction at 100 °C for 12 hours, the vessel was taken out and cooled to room temperature in air.

DC polarization test

A three-electrode system was carried out for DC polarization tests at room temperature on a CHI-660E electrochemical interface: a ZnAl–NO_3 LDH buffer layer-coated Al plate, a ZIF-8 layer-coated Al plate, a ZIF-8–ZnAl–NO_3 LDH layer-coated Al plate or a bare Al plate was used as the working electrode, a platinum filament was used as the counter electrode, and an Ag/AgCl electrode was used as the reference electrode. A 3.5 wt% aqueous solution of NaCl was used as the corrosive medium. Before the test, the samples were immersed in the corrosive medium to measure the open-circuit-potential. The sweep rate and the potential range of the DC polarization test were 10 mV s^{-1} and from -2.0 V to -0.4 V (*vs.* reference), respectively.

Results and discussion

Characterizations of MOF-based anti-corrosion coatings

The first step involved the fabrication of well-intergrown ZnAl–NO_3 LDH buffer layers. Herein, the influence of the reaction temperature and precursor solution composition on the final morphology of the ZnAl–NO_3 LDH precursor coatings was investigated. The optimal reaction conditions for preparing the LDH precursor layer could be determined by a series of experiments with precisely controlled variables. The SEM images indicate that the prepared ZnAl–NO_3 LDH buffer layers exhibit considerable uniformity and compactness under optimized reaction conditions; otherwise, substantial grain boundary defects, which may adversely affect the morphology and anti-corrosion performance of the ZIF-8 coatings, would appear (shown in Fig. 2).

As shown in Fig. 3a, after *in situ* hydrothermal growth, the surface of the Al plates was uniformly covered with close-packed plate-like LDH crystals. Moreover, the LDH crystals were vertically aligned on the Al plates, as could be interpreted by the ‘‘selective evolution’’, a principle proposed by Van der Drift in the interpretation of the preferred orientation of a vapor-deposited PbO layer.[21] The cross-sectional image further

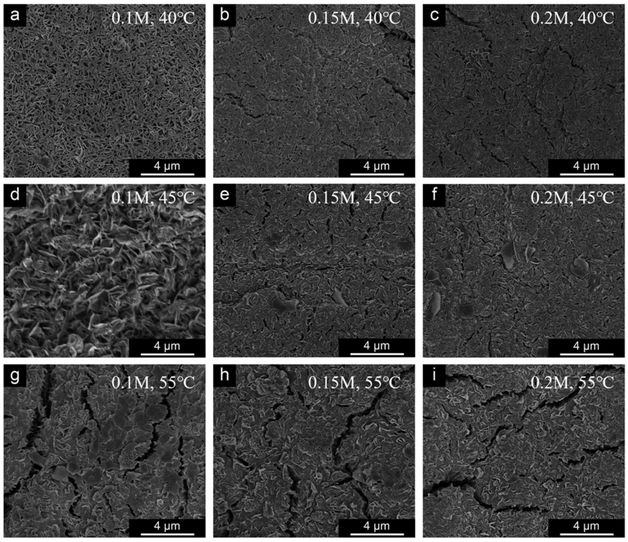

Fig. 2 (a–i) SEM images of ZnAl–NO_3 LDH buffer layers prepared at different temperatures and Zn^{2+} concentrations. All reactions were carried out under identical NH_4NO_3 concentration and the reaction time was fixed at 36 hours.

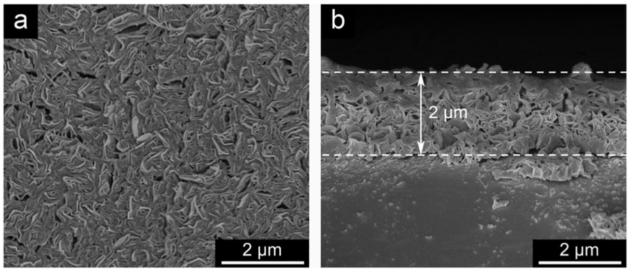

Fig. 3 (a) Top and (b) cross-sectional images of ZnAl–NO_3 LDH buffer layers prepared by *in situ* hydrothermal growth under optimized conditions ([Zn^{2+}]: 0.15 M; reaction temperature: 40 °C; reaction time: 36 h).

demonstrated that the ZnAl–NO_3 LDH buffer layers were uniform with a thickness of 2 μm (Fig. 3b). In addition, the XRD pattern confirmed that the formed coatings indeed belonged to the pure LDH phase with the 2θ value of 10.0°, corresponding to a basal spacing of 8.86 Å, which was characteristic of NO_3^--intercalated ZnAl–LDHs (Fig. 4a).[22,23]

In the next step, the ZnAl–NO_3 LDH buffer layers were further immersed in a methanol solution containing 2-mIm. Our results demonstrated that increasing the concentration of 2-mIm promoted the release rate of Zn^{2+} and the growth rate of the ZIF-8 coatings (shown in Fig. 5). After the solvothermal treatment of the ZnAl–NO_3 LDH buffer layers under optimized conditions, it was found that well-intergrown ZIF-8 coatings with a grain size of 0.5 μm (Fig. 6a) and a thickness of 2.4 μm (Fig. 6b) were formed. Simultaneously, the thickness of the parent ZnAl–NO_3 buffer layers were reduced to 0.45 μm (inset of Fig. 6b). No marginal gap between the ZnAl–NO_3 LDH buffer layers and the ZIF-8 coatings was observed, therefore indicating high-affinity interactions between the ZnAl–NO_3 LDH and ZIF-8 phases. The partial conversion of the ZnAl–NO_3 LDH buffer layers could be attributed to the rapid formation of defect-free protective ZIF-8 surface coatings, which effectively prevented further nucleophilic attack of 2-mIm on the remaining ZnAl–NO_3 LDH buffer layers, as confirmed by our previous research.[24] The formation of the ZIF-8–ZnAl–NO_3 LDH composite coatings was potentially advantageous for the concurrent enhancement in both anti-corrosion and scratch adhesion performances. In addition, the XRD pattern of the prepared coatings (Fig. 4b) indicated that the new emerging diffraction peaks matched well with the standard diffraction pattern of the pure ZIF-8 phase. Nevertheless, it was impossible to accurately identify the diffraction peaks derived from the LDH phase owing to severe peak overlapping between the ZIF-8 and ZnAl–NO_3 LDH phases.

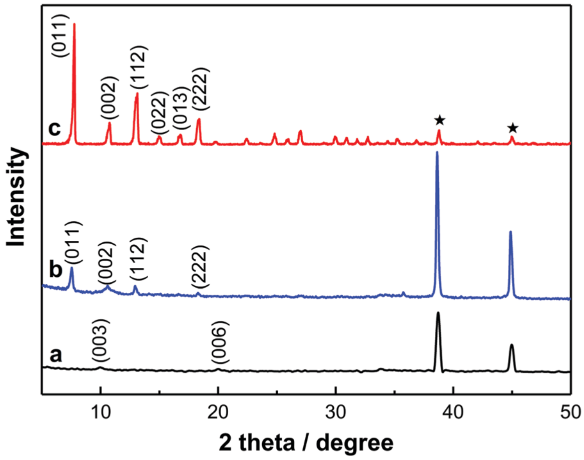

Fig. 4 XRD patterns of (a) ZnAl–NO_3 LDH buffer layer, (b) ZIF-8–ZnAl–NO_3 LDH composite coating and (c) pure ZIF-8 coating; ★ indicates diffraction peaks derived from the Al plate coatings and (c) pure ZIF-8 coatings.

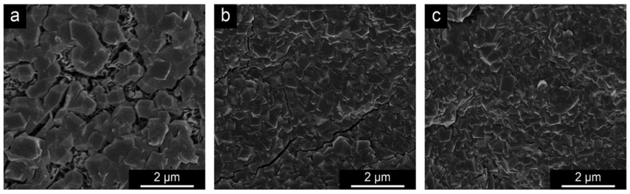

Fig. 5 SEM images of ZIF-8–ZnAl–NO_3 LDH composite coatings prepared at 80 °C for 36 h in methanol with the 2-mIm concentrations of (a) 0.005 g ml^{-1}; (b) 0.01 g ml^{-1} and (c) 0.02 g ml^{-1}.

Besides the above-mentioned experiment, a comparative experiment involving the solvothermal treatment of the ZnAl–NO_3 LDH buffer layers with a precursor solution containing both $Zn(NO_3)_2{\cdot}6H_2O$ and 2-mIm was also conducted. After the solvothermal treatment, it was found that well-intergrown ZIF-8 coatings with a grain size of 5 μm (Fig. 6c), which was significantly larger than that of the above-mentioned ZIF-8–ZnAl–NO_3 LDH composite coatings, were formed. This could be attributed to the much lower nucleation density of the ZIF-8 crystals on the Al plates. Indeed, owing to the slow release of Zn^{2+} from the ZnAl–NO_3 LDH buffer layers and the rapid dissolution of $Zn(NO_3)_2{\cdot}6H_2O$ in the bulk solution, nucleation of the crystal growth of ZIF-8 mainly occurred in the bulk

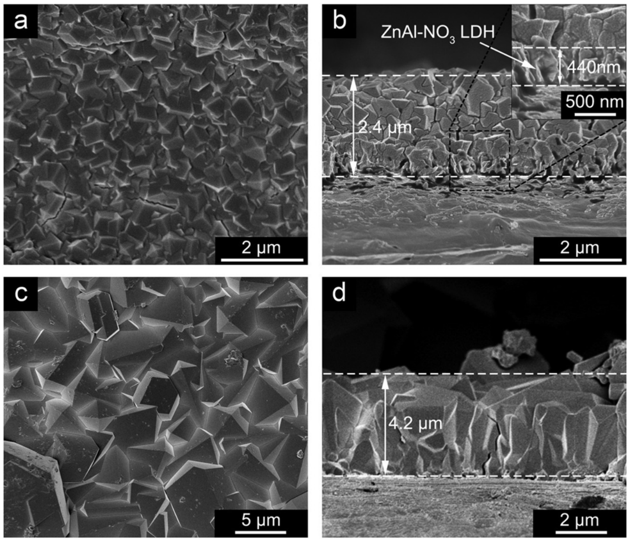

Fig. 6 (a) Top and (b) cross-sectional images of ZIF-8–ZnAl–NO$_3$ LDH composite coatings prepared by ligand-assisted solvothermal conversion of ZnAl–NO$_3$ LDH precursor buffer layers at 80 °C for 36 hours. (c) Top and (d) cross-sectional views of ZIF-8 coatings prepared by "twin zinc source" solvothermal conversion of ZnAl–NO$_3$ LDH precursor buffer layers at 100 °C for 12 hours.

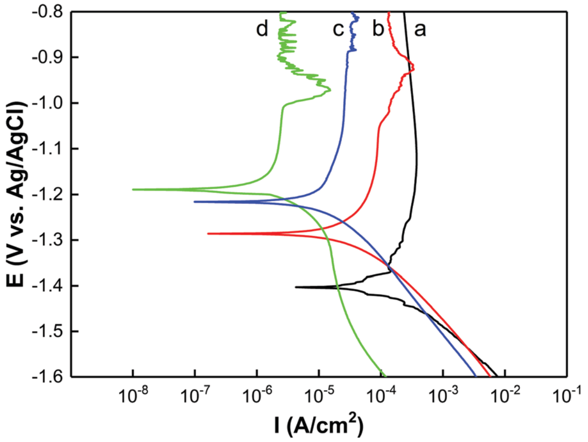

Fig. 7 DC polarization curves for (a) bare Al plates, (b) ZnAl–NO$_3$ LDH buffer layers prepared by *in situ* hydrothermal growth, (c) pure ZIF-8 coatings and (d) ZIF-8–ZnAl–NO$_3$ LDH composite coatings composite coatings.

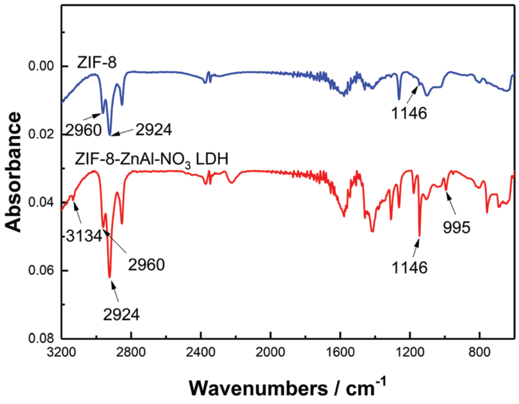

Fig. 8 FT-IR spectra for pure ZIF-8 coatings and ZIF-8–ZnAl–NO$_3$ LDH composite coatings.

solution rather than on the Al plate surface, leading to the formation of the ZIF-8 coatings with a larger grain size and possibly higher grain boundary defect density.[25] Moreover, we noted that after solvothermal treatment, the ZnAl–NO$_3$ LDH buffer layers completely disappeared possibly due to the slow growth rate of the protective ZIF-8 surface coatings, which was incapable of preventing further nucleophilic attack of 2-mIm. In addition, it was noted that the thickness of the ZIF-8 coatings reached 4.2 μm (Fig. 6d), which was attributed to the sufficient supply of nutrients (in particular Zn^{2+}) in the bulk solution.

Evaluation of the corrosion resistance of films

DC polarization represents an effective tool for the evaluation of the performance of anti-corrosion coatings.[25–29] In addition to the ZIF-8 coating-modified Al plates, the anti-corrosion performances of both ZnAl–NO$_3$ LDH coating-modified and bare Al plates were tested for reference. The results indicated that I_{corr} for bare Al plates reached $\sim 10^{-4}$ A cm^{-2} (Fig. 7a). After coating Al plates with the ZnAl–NO$_3$ LDH coatings, I_{corr} was reduced by one order of magnitude: $\sim 10^{-5}$ A cm^{-2} (Fig. 7b). A further large decrease in I_{corr} to $\sim 10^{-7}$ A cm^{-2} was achieved in the case of the ZIF-8–ZnAl–NO$_3$ LDH composite coating-modified Al plates (Fig. 7d), which was superior to that of most MOF-based anti-corrosive coatings[30–34] (a detailed comparison of anti-corrosion performance is summarized in SI-1, ESI†). In contrast, I_{corr} for the ZIF-8 coatings was remarkably higher (Fig. 7c). The superior anti-corrosion performance of the ZIF-8–ZnAl–NO$_3$ LDH composite coatings to that of the pure ZIF-8 coatings could be attributed to the co-existence of the ZnAl–NO$_3$ LDH anti-corrosion coatings and the much higher nucleation density of the ZIF-8 grains on the Al plates, leading to reduced grain boundary defect density. Furthermore, the Fourier transform infrared spectroscopy (FT-IR) results could be used to demonstrate the difference in the grain boundary defect density.[35,36] As shown in Fig. 8, given the similar thickness, the ZIF-8-coated Al plates exhibited significantly weakened absorbances at 995 cm^{-1} (C=C–N twisting), 1146 cm^{-1} (=C–N bending and C–N bending), 2924–2960 cm^{-1} (C–H stretching of CH$_3$), and 3134 cm^{-1} (=C–H asymmetric stretching), indicating the increase in the grain boundary defect density.

The strong adhesion of anti-corrosion coatings to the metal surface is of vital importance for their practical applications.[37] Herein, a scratch test was employed to evaluate the adhesion strength of the ZIF-8–ZnAl–NO$_3$ LDH composite coatings to the Al plates. It was observed that no peeling occurred after scratching the composite coatings with a depth of 40 μm (as shown in SI-2, ESI†), which unambiguously demonstrated their strong adhesion to the Al plates (Fig. 9a and b). In contrast, the pure ZIF-8 coatings were mechanically unstable and could be easily peeled off from the Al plates upon scratching, which was possibly due to the absence of the ZnAl–NO$_3$ LDH phase serving as

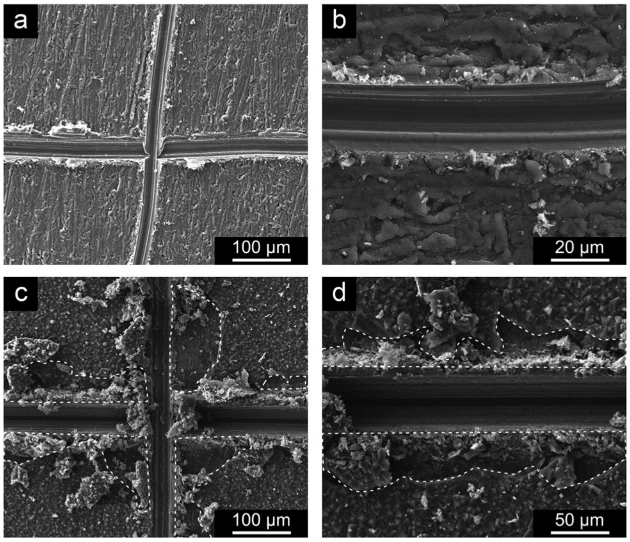

Fig. 9 Evaluation of the adhesion between the ZIF-8–ZnAl–NO_3 LDH composite coatings and Al plates by scratch test. (a) SEM image of the surface morphology of the scratched ZIF-8–ZnAl–NO_3 LDH composite coating and (b) the enlarged image. (c) SEM image of the surface morphology of the scratched pure ZIF-8 coatings and (d) the enlarged image.

the competent gutter layers (Fig. 9c and d). In addition, the prepared ZIF-8–ZnAl–NO_3 LDH composite coatings exhibited considerable thermal stability (as shown in SI-3, ESI†), making them attractive for their use in harsh environments. Considering the structural diversity of water-stable MOF materials,[38–43] it is anticipated that MOF-based composite anti-corrosion coatings with optimized morphology can play an increasingly important role in passivating and protecting metals and their alloys against corrosion.

Conclusions

In summary, relying on a facile partial solvothermal conversion method, we successfully prepared ZIF-8–ZnAl–NO_3 LDH composite coatings on Al plates that exhibited superior anti-corrosion performance and mechanical stability due to the reduced grain boundary defects of the ZIF-8 coatings and the co-existence of the ZnAl–NO_3 LDH anti-corrosion coatings. Taking into consideration both morphological and chemical diversity of water-stable MOFs as well as their excellent compatibility with a wide variety of anti-corrosion materials, it is anticipated that our study can provide new insights into the morphological optimization and performance enhancement of MOF-based anti-corrosion coatings for advancing their practical applications in the future.

Conflicts of interest

The authors declare no conflicts of interest.

Acknowledgements

The authors are grateful to the Thousand Youth Talents Program, National Natural Science Foundation of China (21176231) and the Technology Innovation Team of Dalian University of Technology (DUT2017TB01) for financial support.

Notes and references

1 L. Xia, E. Akiyama, G. Frankel and R. McCreery, *J. Electrochem. Soc.*, 2000, **147**, 2556–2562.
2 S. Pommiers, J. Frayret, A. Castetbon and M. Potin-Gautier, *Corros. Sci.*, 2014, **84**, 135–146.
3 S. H. Zaferani, M. Peikari, D. Zaarei, I. Danaee, J. M. Fakhraei and M. Mohammadi, *Corrosion*, 2012, **69**, 372–387.
4 F. Zhang, L. Zhao, H. Chen, S. Xu, D. G. Evans and X. Duan, *Angew. Chem., Int. Ed.*, 2008, **47**, 2466–2469.
5 T. Yan, S. Xu, Q. Peng, L. Zhao, X. Zhao, X. Lei and F. Zhang, *J. Electrochem. Soc.*, 2013, **160**, C480–C486.
6 Y. Liu, T. Yu, R. Cai, Y. Li, W. Yang and J. Caro, *RSC Adv.*, 2015, **5**, 29552–29557.
7 B. Dou, Y. Wang, T. Zhang, B. Liu, Y. Shao, G. Meng and F. Wang, *J. Electrochem. Soc.*, 2016, **163**, C917–C927.
8 N. Wang, Y. Zhang, J. Chen, J. Zhang and Q. Fang, *Prog. Org. Coat.*, 2017, **109**, 126–134.
9 A. Mesbah, S. Jacques, E. Rocca, M. François and J. Steinmetz, *Eur. J. Inorg. Chem.*, 2011, 1315–1321.
10 C. Wu, Q. Liu, R. Chen, J. Liu, H. Zhang, R. Li, K. Takahashi, P. Liu and J. Wang, *ACS Appl. Mater. Interfaces*, 2017, **9**, 11106–11115.
11 M. Zhang, L. Ma, L. Wang, Y. Sun and Y. Liu, *ACS Appl. Mater. Interfaces*, 2018, **10**, 2259–2263.
12 X. Zhang, Y. Zhang, Y. Wang, D. Gao and H. Zhao, *Prog. Org. Coat.*, 2018, **115**, 94–99.
13 W. Liu, Z. Yan, X. Ma, T. Geng, H. Wu and Z. Li, *Materials*, 2018, **11**, 396.
14 S. E.-d. H. Etaiw, A. E.-A. S. Fouda, S. A. Amer and M. M. El-bendary, *J. Inorg. Organomet. Polym. Mater.*, 2011, **21**, 327–335.
15 I. R. Fernando, N. Daskalakis, K. D. Demadis and G. Mezei, *New J. Chem.*, 2010, **34**, 221–235.
16 M. Deyab, R. Słota, E. Bloise and G. Mele, *RSC Adv.*, 2018, **8**, 1909–1916.
17 D.-M. Zang, D.-K. Cao and L.-M. Zheng, *Inorg. Chem. Commun.*, 2011, **14**, 1920–1923.
18 Y. Li, L. Zhang, X. Xiang, D. Yan and F. Li, *J. Mater. Chem. A*, 2014, **2**, 13250–13258.
19 R. Gao and D. Yan, *Chem. Sci.*, 2017, **8**, 590–599.
20 R. Gao, X. Mei, D. Yan, R. Liang and M. Wei, *Nat. Commun.*, 2018, **9**, 2798.
21 A. Van der Drift, *Philips Res. Rep.*, 1967, **22**, 267.
22 M. Wei, X. Xu, X. Wang, F. Li, H. Zhang, Y. Lu, M. Pu, D. G. Evans and X. Duan, *Eur. J. Inorg. Chem.*, 2006, 2831–2838.
23 L. Wang, C. Li, M. Liu, D. G. Evans and X. Duan, *Chem. Commun.*, 2007, 123–125.
24 Y. Liu, J. H. Pan, N. Wang, F. Steinbach, X. Liu and J. Caro, *Angew. Chem., Int. Ed.*, 2015, **54**, 3028–3032.
25 Q. Fang, Y. Sun, J. Duan, L. Bai, K. Xu, Q. Xiong, H. Xu, K. C.-F. Leung, A. Hui and S. Xuan, *CrystEngComm*, 2019, **21**, 6935–6944.

26 D. E. Beving, A. M. McDonnell, W. Yang and Y. Yan, *J. Electrochem. Soc.*, 2006, **153**, B325–B329.

27 E. Hu, Y. L. W. Huang, Q. Yan, D. Liu and Z. Lai, *Microporous Mesoporous Mater.*, 2009, **126**, 81–86.

28 T. Yu, W. Chu, R. Cai, Y. Liu and W. Yang, *Angew. Chem., Int. Ed.*, 2015, **54**, 13032–13035.

29 R. Cai, M. Sun, Z. Chen, R. Munoz, C. O'Neill, D. E. Beving and Y. Yan, *Angew. Chem., Int. Ed.*, 2008, **47**, 525–528.

30 D. Yu, S. Wen, J. Yang, J. Wang, Y. Chen, J. Luo and Y. Wu, *Surf. Coat. Technol.*, 2017, **326**, 207–215.

31 H. Zhu, W. Hu, S. Zhao, X. Zhang, L. Pei, G. Zhao and Z. Wang, *J. Mater. Sci.*, 2020, **55**, 2215–2225.

32 D.-W. Li, H.-Y. Wang, Y. Liu, D.-S. Wei and Z.-X. Zhao, *Chem. Eng. J.*, 2019, **367**, 169–179.

33 W. Liu, Z. Yan, Z. Zhang, Y. Zhang, G. Cai and Z. Li, *J. Alloys Compd.*, 2019, **788**, 705–711.

34 B. Ren, Y. Chen, Y. Li, W. Li, S. Gao, H. Li and R. Cao, *Chem. Eng. J.*, 2020, **384**, 123389.

35 Y. Dong, Y. Peng, G. Wang, Z. Wang and Y. Yan, *Ind. Eng. Chem. Res.*, 2012, **51**, 3646–3652.

36 P. Cheng and Y. H. Hu, *J. Phys. Chem. C*, 2014, **118**, 21866–21872.

37 M. J. Lee, H. T. Kwon and H.-K. Jeong, *J. Membr. Sci.*, 2017, **529**, 105–113.

38 Y. Liu, L. Li, X. Cai, Q. Chen, M. Xu, Y. Hu, T.-L. Cheung, C. Shek and P. K. Chu, *Thin Solid Films*, 2005, **493**, 152–159.

39 C. Wang, X. Liu, N. K. Demir, J. P. Chen and K. Li, *Chem. Soc. Rev.*, 2016, **45**, 5107–5134.

40 J. Duan, W. Jin and S. Kitagawa, *Coord. Chem. Rev.*, 2017, **332**, 48–74.

41 M. Feng, P. Zhang, H.-C. Zhou and V. K. Sharma, *Chemosphere*, 2018, **209**, 783–800.

42 X. Yang and D. Yan, *Chem. Commun.*, 2017, **53**, 1801–1804.

43 X. Yang and D. Yan, *Chem. Sci.*, 2016, **7**, 4519–4526.